京 都 大 学 防 災 研 究 所 年 報　第47号 C 平成16年3月
Annuals of Disas. Prev. Res. Inst., Kyoto Univ., No. 47 C, 2004

Full-scale Tests for Seismic Performance Verification of Steel Building Structures with Hysteretic Dampers

Praween CHUSILP* and Keiichiro SUITA

* COE Researcher, DPRI, Kyoto University

Synopsis

This paper presents an innovative structural system, named weld-free system, developed to overcome the difficulty in the quality assurance encountered in construction of steel moment resisting frames with conventional welded connections. The proposed structural system adopts a mechanical joint equipped with metallic-yielding damper as beam-to-column connection, wherein slip-critical joints are made by recently developed super high-strength bolts. The structural configuration and load-carrying mechanism of the weld-free system are described herein. Key features of the super high-strength bolts are also introduced. Consequently, two series of experimental verifications of weld-free steel structures are presented. The first series was conducted on three full-scale models of weld-free beam-column subassemblies and one base-line specimen with conventional welded connection. The second series was performed on the whole full-scale three-story weld-free building. The two test series clearly reveal the efficiency of the weld-free system in enhancing large and stable hysteresis loops, while beams and columns above the base can be proportioned to remain elastic under the design earthquakes.

Keywords: steel frames; earthquake resistant structures; connections; weld-free; braces; hysteretic dampers; energy dissipation; cyclic tests

1. Introduction

Among various types of structural materials, steel has long been the most popular in construction of commercial buildings in Japan with the vast majority of low-rise constructions. During the 1995 Hyogoken-Nanbu earthquake, a large number of steel buildings sustained severe damage or even collapsed, notably for low-rise structures (*Reconnaissance,* 1995; Nakashima et al., 1998). One of the most serious damage appeared to be cracks and brittle fracture at welded beam-to-column connections. The damage was inevitable for old steel structures having non-ductile connection details. Damage was also observed in some relatively new buildings designed in accordance with the Japanese seismic codes. Similar to the observation in the U.S. 1994 Northridge earthquake (Youssef et al., 1995), the location where premature fractures initiated was typically in the vicinity of the weld between the beam bottom flange and the column flange.

To assure sufficient plastic deformation capacity of welded beam-to-column connections, several attempts have been made in the U.S. and Japan. After extensive investigations, the reduced beam section design (*Recommended,* 2000) has been widely accepted in the U.S. as an effective and economic solution. On the contrary, based on the observation that cracks often initiated at the toe of the weld access hole, Japanese researchers placed more

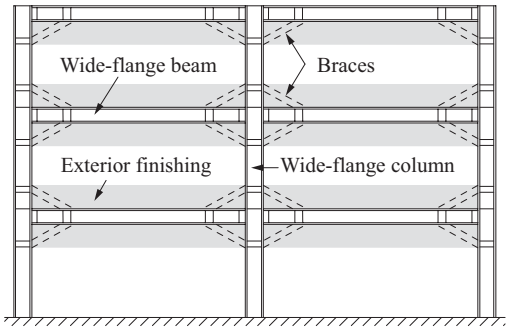

Fig. 1 Configuration of weld-free steel building

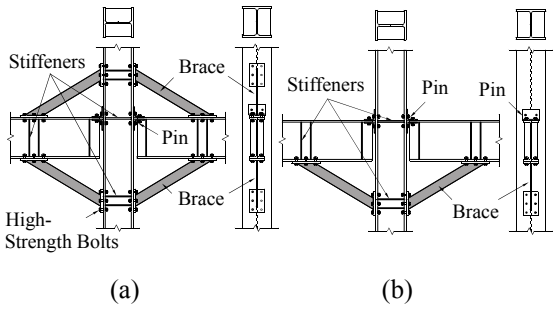

Fig. 2 Weld-free connection details: (a) double-side bracing; (b) single-side bracing

emphasis on connection details to mitigate stress concentrations at welds and finally adopted the connection without weld access hole as an alternative for building construction (*Technical,* 1996). Although these modified connections have shown satisfactory performance in laboratory, it is realized that the quality of welds is difficult to control in practice as long as the structural fabrication relies on workmanship. A recent survey of experimental data of beam-column subassemblies (*Report,* 2000) has confirmed some degree of uncertainty in the quality assurance of welds. Of 339 test specimens reviewed, 30 specimens exhibited premature fracture at welded metals as a result of weld defects. The defects as well as insufficient deposition are often of concern regardless of the connection details adopted. As compared to welded connections in the U.S., the Japanese practice generally requires larger volume of weld, implying that the Japanese connections are more relevant to the quality assurance problems (Nakashima, 2000).

To overcome the difficulty in the weld quality assurance as well as stringent post-Kobe welding requirements, an idea to mainly utilize bolts in beam-to-column connections with the number of welds minimized is appealing. In this regard, an innovative structural system, named 'weld-free' system, is proposed. The distinctive feature of the proposed system is that, with the wide-flange steel adopted for beams and columns, the conventional welded beam-to-column connection is replaced by a mechanical joint equipped with metallic-yielding damper. Super high-strength bolts recently developed are employed to reduce the number of bolts required, thereby permitting smaller cross-sections for the members being joined.

The structural configuration and mechanical characteristics of the weld-free system are addressed in this paper. Furthermore, two series of experimental verification on weld-free steel structures are presented. The first series was conducted on three full-scale weld-free beam-column subassemblies and one base-line specimen with conventional post-Kobe welded connection. The objectives are to verify the seismic performance of the weld-free prototype and to examine the most appropriate weld-free connection details among various possibilities. The second test series was performed on a full-scale three-story weld-free building structure. Testing the whole building allows various complexities, such as the composite action and effects of column base connections, to be considered. The test results are discussed with emphasis on the energy dissipation and damage control efficiency.

2. Structural System

2.1 Structural Configuration

Fig. 1 shows the configuration of the proposed weld-free structural system. Wide-flange beams are bolted to the flanges of wide-flange column only at the top flanges as demonstrated in Fig 2. As a result, the beams rotate about the ends of their top flanges. At the top and bottom of the beam, braces are installed in order to provide the structural system with sufficient lateral resistance against large seismic force and, at the same time, dissipate seismic input energy during a strong earthquake. For buildings with a large number of spans, conventional chevron braces can flexibly be arranged into some spans. However, the great majority of the Japanese construction involves small-scale structures having few spans. A more compact brace is, therefore, introduced to preserve large opening for normal usage [Fig. 2(a)]. In interior frames, large space is required and, thus, the brace may be implemented only at the bottom of the beam [Fig. 2(b)].

A brace of the buckling-restrained type is adopted to prevent overall compression buckling. The buckling-restrained brace developed in this study is more compact than those devised previously (e.g., Watanabe, 1988; Iwata et al., 2000). As shown in Fig. 3, the core plate is made of a steel rectangular bar coated by a friction-reduced material and encased in a restraining sheath made of steel tee section. The sheath can also be built from double steel flat plate whose performance has been verified by a more recent experimental investigation. Each end of the

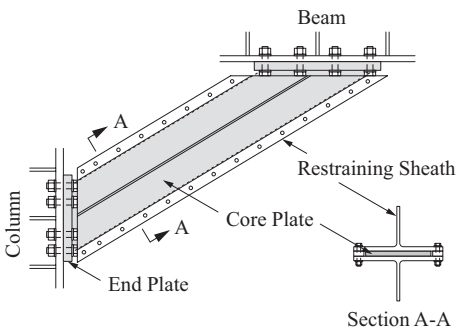

Fig. 3 Details of buckling-restrained brace

core plate is welded to an end plate which, in turn, is bolted to the beam flange or column flange. Welding at the end plate is the only part in this system that requires highly skilled workmanship. To confine axial deformations of the buckling-restrained brace to the core plate, a small gap is provided between the restraining sheath and the end plate so that they do not contact each other when the brace sustains contractions.

The weld-free structural system employs the connection between the beam top flange and the column flange as a means for transferring gravity loads from the beams to the columns. Under a strong ground motion, significant yielding excursion is expected only at the buckling-restrained braces. Beams and columns are designed to respond in the elastic range, except at the base of the structure where plastic deformations may be allowed in the columns. Accordingly, the behavior of the weld-free structural system can be regarded as 'strong column-strong beam-weak brace.'

2.2 Bending Moment Distribution

Fig. 4 presents the bending moment distribution in elastic beams and columns with weld-free connections (solid lines) in comparison to the case of conventional rigid welded connection (dashed line). The weld-free beam-column subassemblies are subjected to a lateral load which produces column shear force Q_c and beam shear force Q_b. Since the flexural stiffness of the brace is very low relative to the beam and column, pin connections are assumed between the beam and the column (point B) and between the brace and the extreme fibers of the beam or column (points A, C, D, and E). The beam has a half length l_b and a depth d_b, while a half story height l_c and a column depth d_c are assumed. The braces incline at an angle α relative to the horizon. Their length is characterized by parameters ξ and ζ as illustrated in the figure.

The moment distribution in beam is coincident in the cases of double- and single-side bracings. The weld-free connection is capable of carrying moment from the beam through a couple of forces exerted on the braces (also on the beam top flange-to-column flange connection for single-side bracing). This moment-carrying mechanism beneficially reduces bending moment in the beam and in some parts of the column, as compared to the moment distribution in the conventional system. The maximum bending moment in beam develops at point D with the magnitude of $(1-\xi)l_bQ_b$. The column moment reaches its peaks at the brace-column junctions. At these locations (points A–D), the discontinuity of bending moment is attributed to the eccentricity between the brace end and the centerline of the beam or column. Since the moment gradient in the column's panel zone (between points A and C for double-side bracing and between points A and B for single-side bracing) is relatively low, shear force induced in the panel zone is reduced significantly. As such, the weld-free connection system does not require a web double plate to reinforce the panel zone. This advantageously allows flexible arrangement of beam-to-column connection details in the column's minor axis.

2.3 Lateral Load-Carrying Mechanism

Weld-free steel frames possess high lateral stiffness due to the presence of buckling-restrained braces. Fig. 5 demonstrates the elastic lateral stiffness of weld-free beam-column subassemblies K normalized by the elastic lateral stiffness of conventional welded beam-column subassemblies K_o. The stiffness K is derived theoretically (see Appendix), assuming interior beam-column subassemblies with the braces inclined at 30 degree relative to the horizon. This brace inclination can

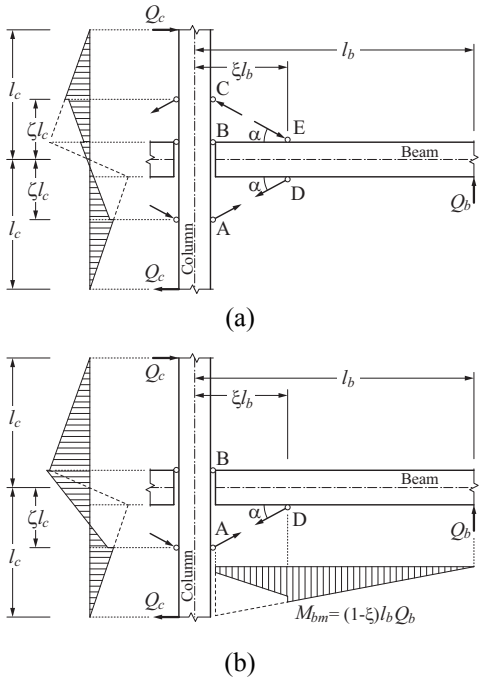

Fig. 4 Moment distribution in weld-free beam-column subassemblies: (a) double-side bracing; (b) single-side bracing

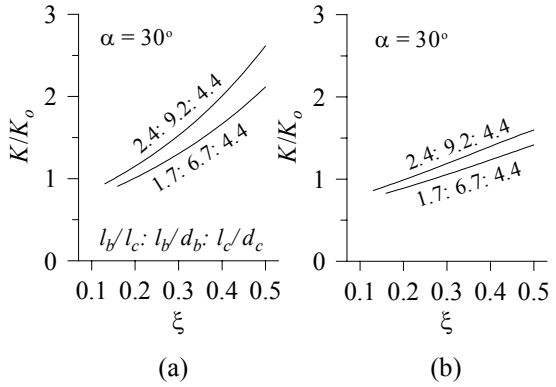

Fig. 5 Elastic lateral stiffness of weld-free beam-column subassemblies: (a) double-side bracing; (b) single-side bracing

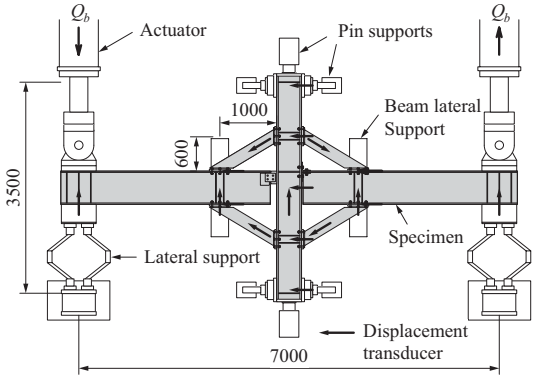

Fig. 6 Setup of weld-free specimen and instrumentation (unit: mm)

appropriately be adopted on a regular basis. The stiffness K_o is computed by considering flexural and shear deformations of the beams and columns as well as shear deformation of the panel zone. Two practical cases characterized by the ratios l_b/l_c: l_b/d_b: l_c/d_c are presented. In each case, the same beam and column cross-sections are used for all weld-free and conventional frames while the cross-sectional area of the braces is determined so that the lateral load-carrying capacity of the weld-free system is identical to that of the conventional system. It is notable that the lateral stiffness of weld-free systems is, in general, insensitive to the change in the axial stiffness of the brace. Fig. 5 clearly reveals that weld-free structures have the lateral stiffness comparable to the conventional frames when single-side bracing is adopted. The weld-free structures can be much stiffer if double-side bracing is implemented. The stiffness is greatly enhanced as the braced length of the beam (characterized by ξ) increases and as the beams and columns become slender.

Presuming that all braces have the same yield force and exhibit elastic-perfectly plastic axial behavior, the lateral load-deformation relationship of weld-free systems is characterized by a bilinear or trilinear curve. For double-side bracing, axial deformation is larger at the bottom brace than the top brace since the center of the rotation at the beam end is located at the beam top flange (point B in Fig. 4). Yielding initiates first at the bottom brace followed by the top brace, leading to trilinear behavior. However, in all practical cases, the second yield force is very close to the first yield force and the behavior of weld-free systems with double-side bracing can be approximated reasonably by the bilinear load-deformation relationship. At the full plastic state, defined at yielding of the top and bottom braces, the theoretical beam shear force is expressed by

$$Q_{bp} = \frac{4\zeta l_c}{2l_b - d_c} N_y \cos\alpha \tag{1}$$

where N_y = tensile yield force of the brace. The column shear force at the full plastic state can then be determined from Q_{bp}.

For single-side bracing, the load-deformation relationship can be represented by a bilinear model. The beam shear force corresponding to yielding of the brace is computed by

$$Q_{bp} = \frac{2\zeta l_c + d_b}{2l_b - d_c} N_y \cos\alpha \tag{2}$$

3 Experimental verification of Weld-Free beam-column subassemblies

3.1 Test Specimens

The tests were aimed at verifying the cyclic performance of the prototype weld-free structures in comparison to a conventional welded moment resisting frame (MRF). A total of four full-scale models of beam-column subassemblies were fabricated. Two specimens are with double-side bracing, designated as D1 and D2, and one specimen is with single-side bracing, designated as S. The only difference between specimens D1 and D2 is the cross-sectional area of the buckling-restrained brace, which was designed to achieve different ratios of the beam's moment demand to its flexural strength. The test results of specimens D1 and D2 would suggest a suitable margin for the design flexural strength of the beam.

In addition to the weld-free specimens, a conventional welded beam-column subassembly, designated as W, was constructed as a base-line specimen. Beams and columns of all specimens have the same lengths as shown in Fig. 6. The chosen cross-sections of the beams and columns were, respectively, wide-flange sections (depth × flange width × web thickness × flange thickness) of $550\times200\times12\times22$ mm and $414\times405\times18\times28$ mm. These cross-sections are typical of low- to medium-rise steel MRFs in Japan.

Table 1 Average Mechanical Properties of Steel Plates

Steel Grade	Sampled Plates	Yield Strength (MPa)	Ultimate Strength (MPa)	Elongation (%)
SN400B	Beam flange	281	429	33
	Beam web	348	455	28
SN490B	Column flange	370	517	27
	Column web	370	508	29
LYP	Brace core	219	301	60

Table 2 Dimensions of Braces and Resulting Load-Carrying Capacities of Beams

Specimen	Dimensions of Brace Core Plate (mm)	N_y (kN)	Q_{cp} (kN)	M_{bm}/M_{by}
D1	130 × 15.5	441	415	0.75
D2	160 × 15.5	543	495	0.92
S	220 × 15.5	747	447	0.83
W	–	–	566	–

Steel grades JIS SN400B and SN490B were selected for the beams and columns, respectively. For the buckling-restrain braces, the core plate was made of commercial low-yield strength (LYP) steel. Mechanical properties of steels obtained from coupon tests of sampled plates are summarized in Table 1. Note that Young's modulus and Poisson's ratio of the LYP steel coincide with those of the conventional structural steels.

(1) Specimens D1, D2, and S

For all weld-free specimens, the braces are horizontally 1000 mm long and incline at 31 degree against the beam centerline. A rectangular bar of 16 mm thick was used as the core plate of the brace. Its width was selected so that the ratio of the maximum bending moment in the beam M_{bm} (equal to $(1-\xi)l_bQ_{bp}$) to the beam yield moment M_{by} (computed by using material properties in Table 2 and the effective beam section to account for the loss of the cross-sectional area due to the bolt holes) is equal to 0.75, 0.92, and 0.83 for specimens D1, D2, and S, respectively. The obtained cross-sectional dimensions of the core plate and the resulting theoretical load-carrying capacities are listed in Table 2. Note that all braces in each specimen have the same dimensions. It could be expected that the beams of specimens D1 and S would respond elastically until the ultimate state, since M_{bm} is limited fairly below M_{by}. On the other hand, with M_{bm} approximately equal to M_{by} the beams of specimen D2 might undergo beyond the proportional limit under large loading.

In the design of buckling-restrained braces, the maximum deformation was conservatively considered at the story drift angle of 0.02 rad which corresponds to two times of the story drift limit commonly considered in the building design against large earthquakes in Japan. The basic design criteria are that at this story drift: (1) yielding concentrates only in the braces while the beams and columns respond elastically; (2) based on observations of past experiments on buckling-restrained braces (e.g., Iwata et al., 2000), axial strain in the core plate may properly be limited within 2% to ensure stable hysteresis behavior under a number of loading cycles; and (3) the restraining sheath remains elastic. The stiffness and strength required for the restraining sheath were determined based on a nonlinear analysis by Inoue et al. (1993, 2001).

Fig. 7 presents the obtained design and connection details of each specimen. Frictions between the core plate and the restraining sheath were avoided by coating the core plate with molybdenum disulfide grease and providing a gap of 0.5 mm between the core plate and the restraining sheath [Fig. 7(d)]. The braces were fastened to the beam flange and column flange by F14T M22 super high-strength bolts (applied tension = 299 kN) through the end plates [Fig. 7(a) and (b)]. The end plates and the adjacent beam flange or column flange were carefully designed so that, until the brace reached its possible maximum force (computed as a product of the core plate's cross-sectional area and the ultimate stress), they remained elastic and no significant slip or bolt prying occurred at the slip-critical joints.

Although the connection between the beam top flange and column flange could be accomplished by double angle, the connection made by a shear plate fasten at the beam web in the vicinity of the beam top flange may be an alternative. In this regard, the right beam of each specimen was joined to the column by double angle connection while the joint at the left

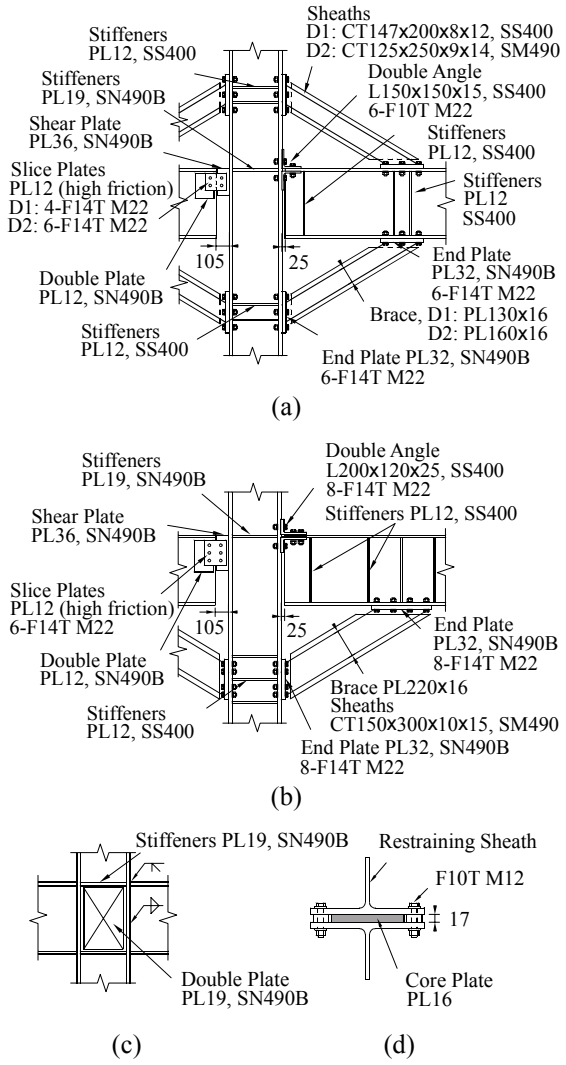

Fig. 7 Connection details (unit: mm): (a) specimens D1 and D2; (b) specimen S; (c) specimen W; (d) buckling-restrained brace

beam was made by a shear plate [Fig. 7(a) and (b)]. The double angle connection requires fillet-welded continuity plates to prevent out-of-plane deformations of the column flanges. On the contrary, continuity plates are not necessary when the shear plate is used to join the beam and column. The shear plate connection, however, requires full penetration groove weld, with careful quality assurance, to attach the shear plate to the column flange. For these two connection types, F14T or F10T high-strength bolts were adopted to produce slip-critical joints. A clearance was provided between the beam and the column to prevent their contact even under the story drift angle of 0.04 rad.

(2) Specimen W

Specimen W was fabricated in accordance with the post-Kobe practice (*Japanese,* 1996; *Technical,* 1996). The beams were shop-welded, without weld access holes, to the column by complete joint penetration welds at the beam flanges and two-sided fillet welds at the beam webs [Fig. 7(c)]. The column flanges were strengthened by continuity plates, and the panel zone was reinforced by a web double plate of 19 mm thick so that the panel zone remains elastic when the full plastic moment develops at the beam ends.

3.2 Loading Setup and Program

The test setup and locations of the displacement measurement relevant to the results discussed herein are as shown in Fig. 6. The column of each specimen was pinned at the tips to the reaction frame, and a hydraulic actuator was mounted to the end of each beam through a clevis. The cyclic story shear was applied quasi-statically to the specimen by means of transverse displacements at the beam tips. The two beams were simultaneously loaded in opposite directions based on an incremental load history containing two cycles of the story drift angle $\theta = 0.02$ rad and subsequent cycles of $\theta = 0.04$ rad applied until the ultimate state. In this study, the ultimate state is defined at which the maximum values of both positive and negative column shear forces are attained. The story drift angle θ is computed in an approximate sense as the ratio of the transverse displacement at the beam tip to the half beam length of 3500 mm. It was expected that testing at the level of $\theta = 0.02$ rad would reveal the performance of the structures under a large earthquake. Loading was, however, applied up to $\theta = 0.04$ rad to explore the structural behavior under an extremely large earthquake.

3.3 Test Results

(1) Hysteresis Behavior

Fig. 8 presents the column shear force Q_c (calculated by $Q_b l_b / l_c$) versus story drift angle θ relationship obtained from the left and right beams of each specimen. The positive sign refers to the loading direction depicted in Fig. 6. For comparison, the theoretical elastic lateral stiffness and the column shear forces at the full plastic state Q_{cp}, derived by means of Eq. (1) or (2) for the weld-free specimens and defined at the beam plastic moment for specimen W, are also plotted. For all weld-free specimens, the predicted initial slope of the load-deformation relationship virtually aligns with the experimental curve. The accuracy of the predicted column shear forces Q_{cp} is also notable. The discrepancy between the theoretical and test results of Q_{cp} is within 10%.

As observed in Fig. 8, all weld-free specimens exhibited stable hysteresis behavior until the ultimate state. The hysteresis loops of the right beams were larger than those of the left beams. This is due to the fact that using double angle to join the beam and column (right beam) would place the center of the beam end rotation right at the end of the top flange.

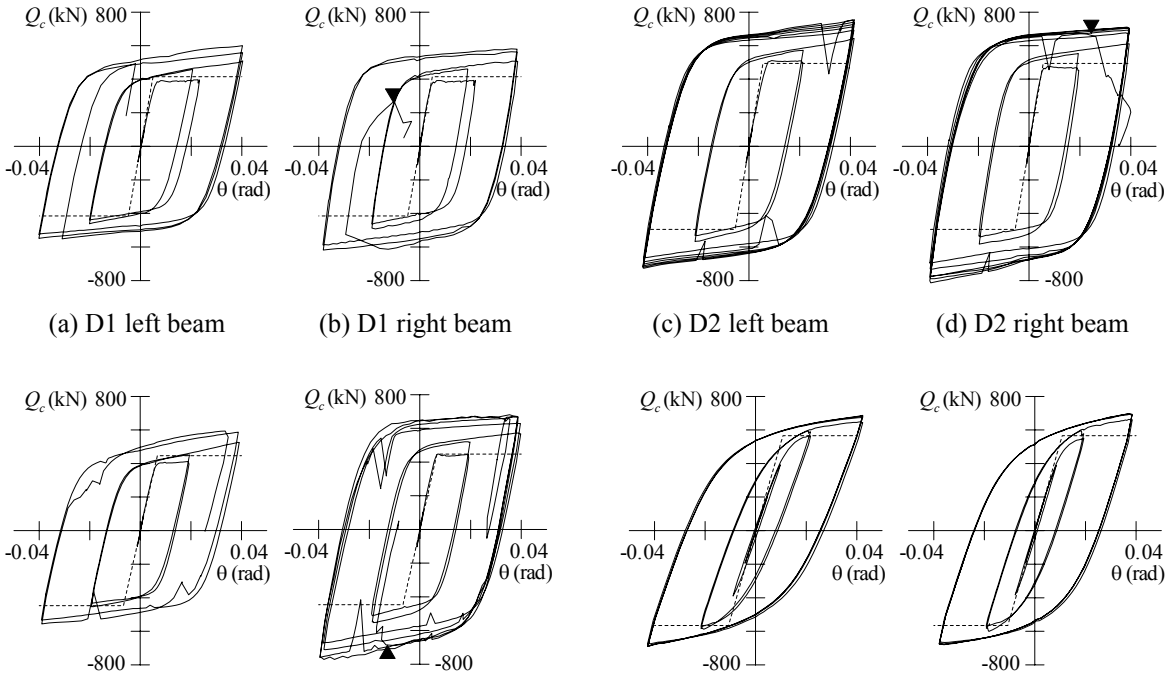

(a) D1 left beam (b) D1 right beam (c) D2 left beam (d) D2 right beam

(e) S left beam (f) S right beam (g) W left beam (h) W right beam

Fig. 8 Column shear force versus story drift angle

On the contrary, the shear plate connection (left beam) located the rotation center at some distance below the beam top flange. The double angle connection, therefore, acquired larger moment arm of the bottom brace's yield force and, thus, greater lateral load-carrying capacity of the structural system.

In 0.02 rad story drift cycles, specimens D1, D2, and S sustained plastic deformation only at the buckling-restrained braces without any signs of damage to other parts of the structures. The strain hardening engaged in the braces at 0.02 rad story drift amplitude caused an increase in the column shear force up to approximately 20%. This hardening should be taken into account in the design to prevent the beams and columns from unexpected plastic deformations. In 0.04 rad story drift cycles, slips occurred at the slip-critical joints in specimens D2 and S and caused an abrupt reduction in the load resistance [Fig. 8(c–f)]. The strength was, however, completely recovered thereafter.

Both specimens D1 and S suffered compression buckling at the core plate of the bottom-right buckling-restrained brace in the vicinity of the end plate, as a consequence of unexpected movement of the restraining sheath which expanded the unrestrained length of the core plate. The buckling occurred in cycles 5 and 7 for specimens D1 and S, respectively, and was followed by fracture at the location of the buckle at the instants marked in Fig. 8(b) and (f). Specimen S also sustained fracture of the super high-strength bolts at the shear plate connection of the left beam, suggesting that the arrangement of bolts at the shear plate should be reviewed to prevent large shear deformation caused by the beam end rotation.

The movement of the restraining sheath was prevented in the test of specimen D2 by penetrating the sheath and the core plate through their thickness with a stud bolt at the mid length of the brace. The prevention of the brace buckling was found to be successful. This enabled specimen D2 to undergo a larger number of cycles under 0.04 rad story drift amplitude. In cycle 9, specimen D2 experienced fracture at the mid length of the core plate in the bottom-right brace and the energy was eventually exploited. The fracture occurred when the brace was loaded in tension at the instant marked in Fig. 8(d).

Unlike the nearly elasto-plastic behavior of the weld-free specimens acquired by uniform yielding in the braces, the behavior of specimen W was characterized by narrow hysteresis loops [Fig. 8(g) and (h)]. Its hysteresis behavior was associated with relatively low elastic stiffness and gradual decrease in the post-yield stiffness as a result of yielding progressed over the beam cross-section. Specimen W attained four cycles of 0.04 rad story drift amplitude before local buckling occurred at both top and bottom flanges of the left and right beams in the vicinity of the welded connection. The panel zone also experienced plastic shear deformation despite the presence of the web double plate. The test was terminated after a reduction in the lateral strength indicating the achievement of the ultimate state.

(2) Energy Dissipation Behavior

The amount of energy dissipated by the weld-free

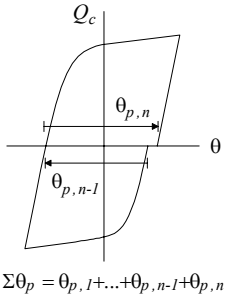

Fig. 9 Definition of cumulative plastic story drift angle

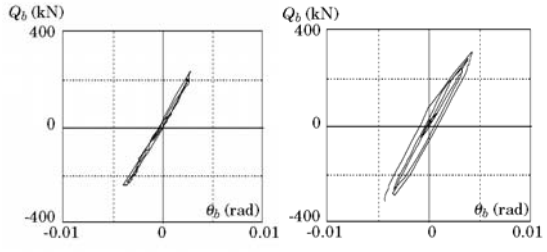

(a) Specimen D1 (b) Specimen D2

Fig. 10 Shear force versus rotation relationship of beams with double angle connections

and conventional systems until the ultimate state is quantified in terms of normalized cumulative plastic story drift angle η, defined as the ratio of the cumulative plastic story drift angle to the theoretical story drift angle at the full plastic state (equal to Q_{cp}/K). The plastic story drift angle is cumulated as described in Fig. 9. Here, the results of the beams with the double angle connections are noted. The parameters η are 85, 152, and 84 for specimens D1, D2, and S, respectively. These values are substantially larger than that of specimen W where η is only 46. This comparison underlines the capability of weld-free systems to achieve greater energy dissipation at the ultimate state than the post-Kobe welded MRFs. The energy dissipation of the weld-free systems may also be superior to the post-Northridge welded MRFs using the reduced beam section connection, since a performance comparison between the post-Kobe and post-Northridge connections (Suita et al., 2000) has evidenced similar amount of the energy dissipation. It is worth noting that, unlike conventional welded MRFs, the energy dissipation and plasticity in the weld-free systems are concentrated only at the braces rather than the beams as will be shown later. These braces can be replaced after an earthquake with more ease than beams and columns.

(3) Plastic Deformation of Braces

To evaluate a degree of plasticity sustained by the buckling-restrained braces, the maximum axial strains of the core plate ε_m are summarized in Table 3. The strain ε_m is determined in the average sense by considering the measured elongation of the core plate. As expected, the bottom braces of all weld-free specimens underwent larger axial strains than did the top braces. The maximum axial strains of the bottom braces are found to be 3.0 to 3.5% at the applied story drift angle of 0.04 rad (before the cycles of fracture). At 0.02 rad story drift angle which was considered in the design of the braces, the maximum axial strains were approximately 50% smaller and fairly below the design strain limit of 2%.

Table 3 Summary of Deformations and Failure Mode of Braces at Beams with Double Angle Connections

Specimen	Bracing Side	ε_m (%)	η_d	Failure Mode
D1	Top	1.88	194	–
	Bottom	3.48	378	local buckling
D2	Top	1.65	331	–
	Bottom	3.28	639	tensile fracture
S	Bottom	3.03	495	local buckling

Table 3 also presents the normalized cumulative plastic axial deformation η_d of the braces at the beams with double angle connections. The index η_d is defined as the ratio of the cumulative plastic axial deformation of the core plate (computed in a similar manner as illustrated in Fig. 9) to its yield axial displacement. The most notable value of η_d is observed at the bottom brace of specimen D2 where η_d is as high as 639. This result discloses the effectiveness of the developed buckling restraining system in preventing severe buckling of the core plate, leading to a large amount of the energy dissipation. The index η_d is significantly smaller for specimens D1 and S. However, provided that premature buckling of the braces was properly prevented, the deformation capacity of these two specimens should be increased considerably.

(4) Plastic Deformation of Beams

Control of damage in primary structural members is an important issue that reflects the efficiency of damage control systems. The damage to the test specimens is evaluated by means of plastic deformation sustained by the beams. Fig. 10 shows examples of the shear force-rotation relationship of the beams with double angle connections obtained from specimens D1 and D2. Here, θ_b denotes the rotation of the unbraced beam portion, derived by dividing the relative transverse displacement between the beam tip and the beam-brace junction (caused by flexural and shear deformations of the beam) by the unbraced beam length. The plot clearly demonstrates essentially elastic response of specimen D1. The beam of specimen D2 experienced some yielding as a

result of substantial strain hardening engaged in the braces. However, such plasticity is apparently insignificant. This observation suggests that weld-free structures can be designed by providing the beams with the yield moment equal to the maximum bending moment induced in the beams. Accordingly, plastic deformations will be concentrated only in the braces (possibly with slight yielding in the double angle connection) while the beams and columns respond nearly in the elastic range until the ultimate state of the structure.

4 Full-Scale Tests of Weld-Free Steel Building Structure

An extensive experimental verification was conducted on a full-scale three-story weld-free building structure at Katsura Int'tech Center of Kyoto University. The primary objective is to verify the constructability, seismic performance, and collapse mechanism of weld-free structures under bilateral loading. Testing the whole building allows various complexities, including the composite action, effects of column base connection, and moment redistribution, to be accounted for. Although the experimental data is still being processed, the results reported herein are adequate to demonstrate the actual application and key behaviors of weld-free building structures.

4.1 Geometry and Materials of Building Specimen

Figure 11 shows a general view of the building specimen, whose elevation and floor plans are presented in Fig. 12. The dimensions adopted for the frame are typical of low- to medium-rise construction in Japan. The frame has two bays of 6.00 m wide in the E-W direction and one bay of 8.25 m wide in the N-S direction. Each story is 3.50 m high, except in the third story where the columns were constructed up to the inflection points (1.50 m from the second floor). At the column tips, a strong horizontal bracing system was installed to simulate the rigid diaphragm action as well as to support hydraulic actuators.

Fig. 11 General view of building specimen

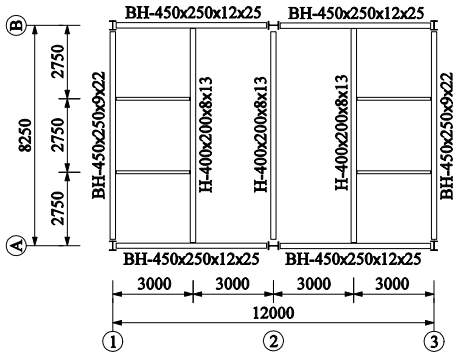

(a) Plan of floors 2 and 3

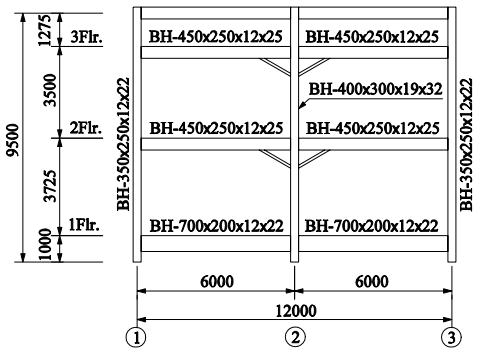

(b) Elevation of E-W frame

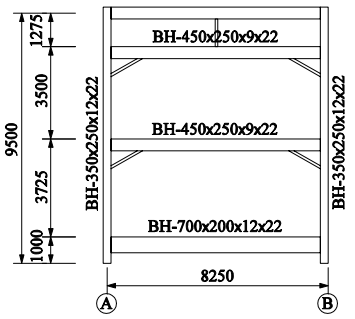

(c) Elevation of exterior N-S frame

Fig. 12 Elevation and floor plan of building specimen (unit: mm)

The alignment of the columns is as shown in Fig. 12(a). In the column's strong axis, the adopted beam-to-column connection is presented in Fig. 13. The joint between the beam top flange and column flange was made by double angle, whose performance under large beam rotations has been verified. The buckling-restrained brace used in the building specimen is similar to that introduced previously. An exception is that the restraining sheath was built up from double flat plates (see Fig. 13).

In the column's weak axis, some difficulty may arise in configuring the buckling-restrained braces into the connection. Preference is, therefore, given to the use of a simple pinned connection which employs bolted splices at the beam top flange, as a means for transferring shear forces, and a thin plate at the beam

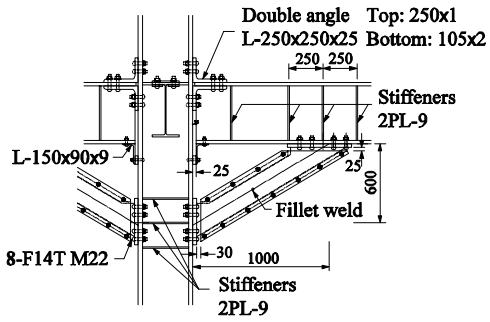

(a) Connection details

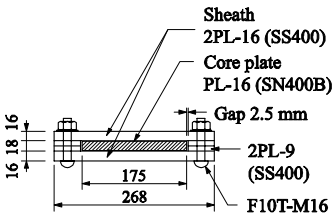

(b) Cross-section of buckling-restrained brace

Fig. 13 Beam-to-column connection in column strong axis

bottom flange to improve the lateral-torsional stability of the beam. At the column bases, strong wide-flange steel foundation beams were bolted to the column through tee stubs in the column's strong axis and through splice plates in the column's weak axis.

Steel grade SS400 was selected for both beams and columns, while the core plates of the braces were made of SN400B steel. The material properties obtained from coupon tests are summarized in Table 4. At each floor, reinforced concrete (RC) slabs of 165 mm thick were constructed in a traditional manner and were partially connected to the primary beams by shear studs. The ultimate compressive strength of 21 MPa was chosen for the concrete.

4.2 Design Criteria

Weld-free structures can be designed rationally by considering the buckling-restrained braces as primary lateral load-resisting members, while their energy dissipation can be treated as a secondary effect. The building specimen was designed with regard to the lateral story shear of 750 kN applied in both longitudinal and transverse directions. The story weight of 550 kN was assumed at each floor. The shear force exerted on each column was estimated by presuming that the column resists lateral load in the strong axis only. The bending moment distribution in beams and columns was consequently computed from the column shear forces.

Axial forces sustained by the braces were determined based on the static equilibriums. With the cross-section of 175×16 mm chosen for all core plates, the beams would remain elastic when the braces sustain significant plastic deformations. To prevent overall buckling of the core plate, the restraining sheath was designed in accordance with Inoue et al. (1993, 2001). Beams were proportioned with regard to the moments, induced by bilateral loading, superimposed with the moments due to gravity loads. The latter can be computed with the assumption of simply supported beams, since the braces will be installed so that their contribution to the gravity load-carrying mechanism of the frame is minimized. The beams and columns were designed to remain elastic when the braces and column bases (immediately above the foundation beams) reach the full plastic state. The finally obtained cross-sections of the primary structural members are as described in Fig. 12. Note that the built-up wide-flange section is denoted by BH in the figure.

4.3 Test Setup and Loading Program

Due to the presence of strong foundation beams, the building specimen would not transfer moment to the foundation. The specimen was, therefore, simply placed on the reaction floor with only 'shear keys' provided to prevent horizontal displacements of the

Table 4 Average material properties of building specimen obtained from coupon tests

Member	Plate thickness (mm)	Steel grade	Yield stress (MPa)	Ultimate stress (MPa)	Elongation (%)
Column	12	SS400	298	415	34
	19	SS400	276	425	33
	22	SS400	271	419	34
	32	SS400	253	415	36
Floor beam	9	SS400	292	422	31
	12	SS400	298	415	34
	22	SS400	276	420	34
	25	SS400	249	410	34
Foundation beam	22	SS400	276	420	34
Brace core plate	16	SN400B	289	428	33
Split tee	19	SM490A	331	510	28

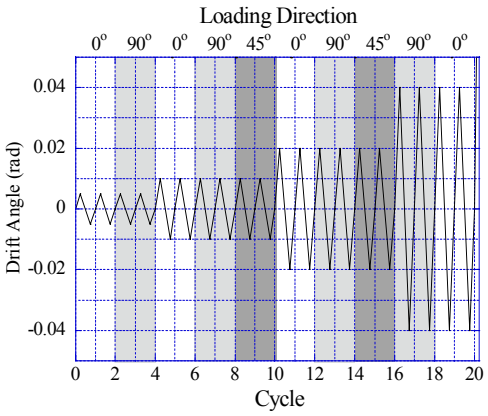

Fig. 14 Loading history applied to building specimen

frame at the ground level. Presuming that higher vibration modes are not prominent, lateral loads were applied only at the top of the frame through two long stroke hydraulic actuators, mounted to the horizontal bracing system at the mid longitudinal and mid transverse lengths. The loading capacity of each actuator is 3000 kN for pushing and 1500 kN for pulling.

Lateral loads were generated quasi-statically so as to simulate the unilateral and bilateral earthquake loadings. The unilateral loading was performed by a single actuator in either N-S or E-W direction (referred to as 0^o and 90^o loadings, respectively), while the bilateral loading was conducted by means of top displacements equally applied in two directions (45^o loading). The loading history is presented in Fig. 14. The applied deformation amplitudes include 0.005, 0.01, 0.02, and 0.04 rad drift angles (computed as top displacement divided by the total frame height of 9500 mm). The specimen was subsequently pushed in the 0^o direction to explore the collapse mechanism.

4.4 Test Results

Figure 15 shows the lateral force versus drift angle relationship obtained from 0^o, 90^o, and 45^o loadings. Under 0^o and 90^o loadings, the building specimen exhibited large and stable hysteresis loops even under the drift angle of 0.04 rad, being four times of the deformation level considered in the design against strong earthquakes. The lateral load-carrying capacity is greater than 1500 kN, although only four buckling-restrained braces were provided at each floor in the longitudinal and transverse directions.

Because the columns would sustain significant stresses under bilateral loading, the applied drift angle was limited to 0.02 rad. The E-W and N-S components of the applied loads, determined with geometrical nonlinearity considered, are as shown in Fig. 15 (c) and (d). Stable hysteresis behavior is also

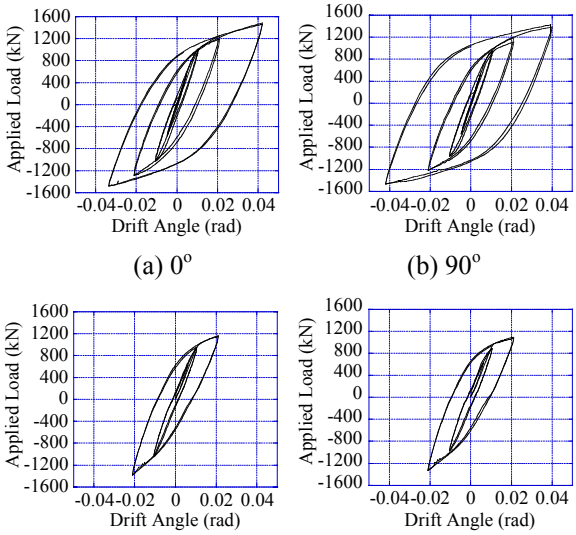

Fig. 15 Lateral force versus drift angle relationship

obtained in this case. Experimental observations suggest that caution should be taken in the foundation design of weld-free building structures to prevent excessive uplift displacements caused by overturning moments under bilateral loading.

An example of the hysteresis curves of the buckling-restrained braces is presented in Fig. 16. This result is obtained from the brace at column A-1 (see Fig. 12(a)) in the second floor under 90^o loading. The axial force is determined from the beam moments, while the axial strain is computed from the measured elongation and contraction of the core plate. It can be seen that the load-deformation curve of the brace is close to the idealized bilinear behavior. The brace exhibited stable hysteresis response with a large amount of energy dissipated. The behavior of the other buckling-restrained braces is also similar to the result shown in Fig. 16.

In all cyclic tests, there was no sign of damage observed in the building, except extensive cracks of RC slabs and plastic deformations in the braces and column bases. Some plastic shear deformations were also observed in the panel zone of the columns in the cycles with 0.02 rad drift angle. In the final test, the

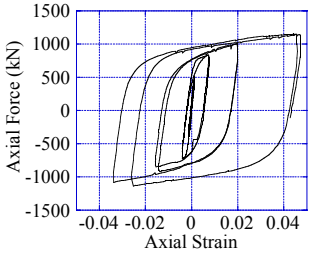

Fig. 16 Axial force versus axial strain relationship of buckling-restrain brace

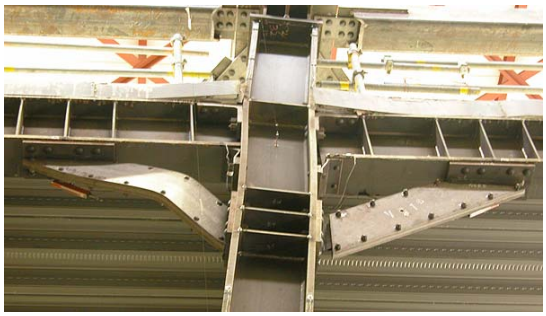

Fig. 17 Shear yielding of column panel zone and buckling of buckling-restrain brace at second floor of south plane frame

specimen was monotonically pushed to failure. The collapse mechanism developed as a consequence of overall buckling of the brace at the first floor of the south plane frame, which was shortly followed by buckling of the other brace at the second floor of the same frame (see Fig. 17). The test was terminated after the buckling of these braces. The maximum drift angle attained by the specimen is as large as 0.10 rad.

5 Conclusions

The innovative weld-free structural system has been presented in this paper. The proposed system was developed to overcome the quality assurance problem as well as stringent requirements encountered in construction of welded MRFs. The seismic performance of the weld-free system has been verified by cyclic tests on four full-scale beam-column subassemblies and one full-scale three-story weld-free building. The primary findings and conclusions can be drawn as follows:

[1] Weld-free structures exhibit stable hysteresis behavior under the deformation of four times larger than the level considered in the design against large earthquakes. Their hysteresis loops appear to be considerably larger than those of the conventional welded MRFs.

[2] The weld-free beam-to-column connection limits plastic deformations essentially in the buckling-restrained braces. The beams remain virtually elastic, while the columns may sustain some shear yielding in the panel zone.

[3] The column base of weld-free structures can be accomplished by bolting strong foundation steel beams to the column flanges. The developed column base connection confines plastic hinges in the columns and, thus, enhances the ductility and energy dissipation of the structure.

[4] The capability to limit plastic deformations at key locations advantageously increases the ductility capacity of weld-free structures. The structures collapse in a ductile mode and can attain the maximum drift angle of as large as 0.10 rad.

The comprehensive experimental verification presented herein has verified excellent seismic performance of weld-free building structures. The proposed structural system can now be adopted with confidence in the full-scale application.

Acknowledgments

This research was supported by the Ministry of Education, Culture, Sports, Science, and Technology of Japan (No. 12555159 and 13305037 for the subassembly and building tests, respectively). Prof. Kazuo Inoue of Kyoto University served as the principal investigator. His support is gratefully acknowledged. The authors are also grateful to Dr. N. Uno and I. Takeuchi of Nippon Steel Corporation for their technical support in the subassembly tests and to Prof. M. Nakashima, Y. Koetaka, Y. Byakuno, and M. Ando of Kyoto University, T. Tanaka and Y. Sawai of Takenaka Corporation, and K. Taga and Y. Tashiro of Nikken Sekkei Corporation for their contributions and participation in the building tests.

References

Hirai, K., Wakiyama, K., Uno, N., and Miyagawa, T. (2002): Experimental study on delayed fracture of high strength bolt (Part 2 Exposure tests), *J. Struct. Constr. Eng.*, AIJ, 555, pp. 171-176 (in Japanese).

Inoue, K., Chang, P. Y., Mine, T., Hukuyama, K., and Inoue, K. (1993): Stiffening design of the precast concrete panels to prevent the steel flat braces from buckling, *J. Constr. Steel*, JSSC, 1, pp. 195-202 (in Japanese).

Inoue, K., Sawaizumi, S., and Higashibata, Y. (2001): Stiffening requirements for unbonded braces encased in concrete panels, *J. Struct. Eng.*, ASCE, 127(6), pp. 712-719.

Iwata, M., Kato, T., and Wada, A. (2000): Buckling-restrained braces as hysteretic dampers, *Proc. Third Inter. Conf. on Behavior of Steel Struct. in Seismic Areas (STESSA 2000)*, Montreal, pp. 33-38.

Japanese Architectural Standard Specification: JASS 6 Steel Work. (1996): AIJ, Tokyo (in Japanese).

Nakashima, M. (2000): Quality assurance for welding of Japanese welded beam-to-column connections, *Proc. Third Inter. Conf. on Behavior of Steel Struct. in Seismic Areas (STESSA 2000)*, Montreal, pp. 223-230.

Nakashima, M., Inoue, K., and Tada, M. (1998): Classification of damage to steel buildings observed in the 1995 Hyogoken-Nanbu earthquake, *Eng. Struct.*, 20(4-6), pp. 271-281.

Recommended seismic design criteria for new steel moment-frame buildings. (2000): FEMA350,

Federal Emergency Management Agency, Washington, D.C.
Reconnaissance report on damage to steel building structures observed from the 1995 Hyogoken Nanbu earthquake. (1995): Kinki Branch, AIJ, Osaka (in Japanese).
Report of survey and research on steelworks. (2000): Managing Committee of Structural Steelwork, AIJ (in Japanese).
Suita, K., Nakashima, M., and Engelhardt, M. D. (2000): Comparison of seismic capacity between post-Northridge and post-Kobe beam-to-column connections, *Proc. Third Inter. Conf. on Behavior of Steel Struct. in Seismic Areas (STESSA 2000)*, Montreal, pp. 271-278.
Technical recommendations for steel construction for buildings. Part 1 Guide to steel-rib fabrications. (1996): AIJ (in Japanese).
Wakiyama, K. (2001): Development of super-high tension bolt, *JSSC Bulletin*, JSSC, 40, pp. 47-51 (in Japanese).
Watanabe, A., Hitomi, Y., Saeki, E., Wada, A., and Fujimoto, M. (1988): Properties of brace encased in buckling-restraining concrete and steel tube, *Proc. Ninth World Conf. on Earthquake Eng.*, Tokyo-Kyoto, IV, pp. 719-724.
Youssef, N. F. G., Bonowitz, D., and Gross, J. L. (1995): A survey of steel moment resisting frame buildings affected by the 1994 Northridge earthquake, NISTIR 5625, National Institute of Standards and Technology, Gaithersburg, MD.

Appendix

The elastic lateral stiffness of a weld-free beam-column subassembly K, defined as the column shear force divided by the story drift angle, can be expressed by

$$K^{-1} = K_d^{-1} + K_b^{-1} + K_c^{-1} \tag{A1}$$

where K_d, K_b, and K_c = lateral stiffness that relates the column shear force to a component of the story drift angle caused by deformations of the braces, beams, and columns, respectively. For weld-free systems with double-side bracing, an extensive study shows that in estimating the stiffness the eccentricity at the beam end (point B in Fig. 4) is negligible, while eccentricities at points A, C, D, and E should be taken into account. Applying the principle of virtual forces, each term in Eq. (A1) can be obtained:

$$K_d = \frac{8nA_d E l_c (\zeta l_b \cos\alpha)^2 \sin\alpha}{(2l_b - d_c)^2 (2\zeta l_c - d_b)} \tag{A2}$$

$$K_b = n\left[\frac{8l_b l_c^{\,2}(1-\xi)^3 + C_1^{\,2}(2\xi l_b - d_c)^3}{12 l_c E I_b} + \frac{2l_c^{\,2}(1-\xi) + C_1^{\,2} l_b (2\xi l_b - d_c)}{l_b l_c G A_{bw}}\right]^{-1} \tag{A3}$$

$$K_c = \left[\frac{3C_1^{\,2} d_c^{\,2}\zeta - 6C_1 C_2 d_c l_c \zeta^2}{12 E I_c} + \frac{l_c^{\,2}(1 - 3\zeta + 3\zeta^2 + (C_2^{\,2} - 1)\zeta^3)}{3EI_c} + \frac{1 + \zeta(C_2^{\,2} - 1)}{GA_{cw}}\right]^{-1} \tag{A4}$$

$$C_1 = \frac{(2l_b - d_c)}{2\zeta l_b}\tan\alpha - \frac{l_c}{l_b}\,;$$

$$C_2 = \frac{2l_b(1-\zeta) - d_c}{2\zeta l_b} \tag{A5}$$

where n = 1 and 2 for exterior and interior beam-column subassemblies, respectively, having a half beam length l_b and a haft story height l_c; I_b and I_c = moments of inertia of the beam and column, respectively; A_d, A_{bw}, and A_{cw} = cross-sectional areas of the brace, beam web, and column web, respectively; and E and G = Young's and shear moduli, respectively.

For weld-free systems with single-side bracing, the eccentricity at the beam end needs to be considered. The lateral stiffness is written by:

$$K_d = \frac{nA_d E l_b^{\,2}(2\zeta l_c + d_b)^2 \cos^2\alpha \sin\alpha}{l_c (2l_b - d_c)^2 (2\zeta l_c - d_b)} \tag{A6}$$

$$K_b = n\left[\frac{3C_3^{\,2} d_b^{\,2}(2\xi l_b - d_c) + 3C_3 C_4 d_b (2\xi l_b - d_c)^2}{12 l_c E I_b} + \frac{C_4^{\,2}(2\xi l_b - d_c)^3}{12 l_c E I_b} + \frac{2l_b l_c (1-\xi)^3}{3EI_b} + \frac{2l_c^{\,2}(1-\xi) + C_4^{\,2} l_b (2\xi l_b - d_c)}{l_b l_c G A_{bw}}\right]^{-1} \tag{A7}$$

$$K_c = \left[\frac{(2l_c - d_b)^3 - 8l_c^{\,3}(\zeta - 1)^3}{48 l_c E I_c} + \frac{(8C_5^{\,3} + (C_6 d_b + 2C_6 l_c \zeta - 2C_5)^3)/C_6}{48 l_c E I_c} + \frac{d_b(C_6^{\,2} - 1) + 2l_c(2 + \zeta(C_6^{\,2} - 1))}{4 l_c G A_{cw}}\right]^{-1} \tag{A8}$$

$$C_3 = \frac{l_c(2l_b - d_c)}{l_b(2\zeta l_c + d_b)}\,;\; C_4 = C_3\tan\alpha - \frac{l_c}{l_b}\,;$$

$$C_5 = l_c(1-\zeta) - C_3 d_c \tan\alpha\,;\; C_6 = 2C_3 - 1 \tag{A9}$$

要 旨

建築構造物の耐震改修・再生に活用できる履歴ダンパーの効用を実証する実大構造物実験に取り組んだ. 地震エネルギーの吸収能力の高さが既に実証されている座屈拘束型のダンパーを使い, 施工時の接合品質が安定した高力ボルト接合を主体とした新しい構造形式が提案されており, これを用いた柱梁接合部を対象とする部分架構と, 3層の実大立体骨組を対象とする2つの実験プロジェクトに取り組み, その力学挙動と耐震性能を検証した.

キーワード : 鋼構造建物, 耐震性能, 履歴型ダンパー, 座屈拘束ブレース, 施工品質